InP quantum dots: Electronic structure, surface effects, and the redshifted emission

Huaxiang Fu and Alex Zunger
National Renewable Energy Laboratory, Golden, Colorado 80401
(Received 16 December 1996)

We present pseudopotential plane-wave electronic-structure calculations on InP quantum dots in an effort to understand quantum confinement and surface effects and to identify the origin of the long-lived and redshifted luminescence. We find that (i) unlike the case in small GaAs dots, the lowest unoccupied state of InP dots is the Γ_{1c}-derived direct state rather than the X_{1c}-derived indirect state and (ii) unlike the prediction of $\mathbf{k}\cdot\mathbf{p}$ models, the highest occupied state in InP dots has a $1sd$-type envelope function rather than a (dipole-forbidden) $1pf$ envelope function. Thus explanations (i) and (ii) to the long-lived redshifted emission in terms of an orbitally forbidden character can be excluded. Furthermore, (iii) fully passivated InP dots have no surface states in the gap. However, (iv) removal of the anion-site passivation leads to a P dangling bond (DB) state just above the valence band, which will act as a trap for photogenerated holes. Similarly, (v) removal of the cation-site passivation leads to an In dangling-bond state below the conduction band. While the energy of the In DB state depends only weakly on quantum size, its radiative lifetime increases with quantum size. The calculated ~300-meV redshift and the ~18 times longer radiative lifetime relative to the dot-interior transition for the 26-Å dot with an In DB are in good agreement with the observations of full-luminescence experiments for unetched InP dots. Yet, (vi) this type of redshift due to surface defect is inconsistent with that measured in *selective* excitation for HF-etched InP dots. (vii) The latter type of (''resonant'') redshift is compatible with the calculated *screened* singlet-triplet splitting in InP dots, suggesting that the slow emitting state seen in selective excitation could be a triplet state. [S0163-1829(97)04428-7]

I. INTRODUCTION

One of the interesting features of the spectroscopy of quantum dots is the almost universal occurrence of a redshift of the emission relative to the absorption. This was seen in quantum dots of Si,[1–6] CdSe,[7–15] InP,[16,17] and InGaAs (Refs. 18 and 19) and exists irrespectively of the preparation methods of the dots, whether it is based on colloidal chemistry[7–17] or on strain-induced dot formation.[18,19] One obvious reason for the redshift is the existence of a residual size distribution even in the best prepared dot samples: The larger dots in a sample have lower band-edge energies [horizontal lines in Fig. 1(a)], so if one excites a sample with sufficiently-high-energy photons above the band edge of the smallest dot [a ''global excitation'' experiment; see Fig. 1(c)], the emission will be redshifted because it results from the deexcitation of band edges of *all* the dots in the sample. The corresponding size-dependent ''nonresonant Stokes shift'' Δ_{nonres}, the difference between the lowest-energy peak in the absorption spectra and the emission peak [see Fig. 1(c)], is large [~100 meV in CdSe (Ref. 13) and ~200 meV for InP (Refs. 16 and 17)]. It is possible, however, to eliminate much of the effect of size distribution by exciting selectively only the largest dots in a sample, using sufficiently-low-energy photons. Such a ''selective excitation'' experiment [also called ''fluorescence line narrowing'' (FLN); see Fig. 1(d)] gives the ''resonant Stokes shift'' Δ_{res}, the energy difference between the excitation line and the FLN emission peak, which reflects an intrinsic redshift of a given dot. Interestingly, (i) this type of redshift is usually accompanied by an emission having a rather long lifetime [e.g., ~1 μsec at 10 K for CdSe (Ref. 10) and 0.5 μsec at 10 K for InP (Ref. 17)] relative to that of conventional allowed bulk transition and (ii) the larger the size of the dot, the smaller[12,17] the redshift Δ_{res}. These observations regarding the slow, redshifted emission can be cast phenomenologically in terms of a schematic energy-level diagram shown in Fig. 2, where $|g\rangle$ indicates the ground state (electrons are not removed from valence states), while the two excited electron-hole states $|E_{\text{fast}}\rangle$ and $|E_{\text{slow}}\rangle$ denote, respectively, the fast, high-energy *allowed* state and the slow, redshifted *forbidden* state. Given the almost universal existence of a slow, redshifted emission in different semiconductor quantum dots, with a reduced redshift as the dot becomes larger, many studies have aimed at identifying the origin and nature of the excited states $|E_{\text{slow}}\rangle$ and $|E_{\text{fast}}\rangle$. Four models have been suggested to explain the nature of the state $|E_{\text{slow}}\rangle$.

(i) Intrinsic, spin-forbidden state. In this hypothesis, the electron-hole exchange interaction,[1,13,20,21] normally negligible in bulk semiconductors (~1 meV),[22] is assumed to be sufficiently enhanced in small quantum structures so as to significantly split the electron-hole state into a lower energy, *spin-forbidden* component $|E_{\text{slow}}\rangle$ (e.g., triplet or quintuplet) and a higher-energy, *spin-allowed* component $|E_{\text{fast}}\rangle$ (e.g., singlet). The observed emission versus absorption redshift is then the exchange splitting[21] and the long lifetime of the emission from $|E_{\text{slow}}\rangle$ to the singlet $|g\rangle$ is attributed to the spin-forbidden character of $|E_{\text{slow}}\rangle$ with respect to the ground state $|g\rangle$. This model has been applied to explain the ''red emission'' in porous Si by Calcott *et al.*[1] It explains the ~10-meV redshift and the crossover from a long lifetime at low temperature (emission from $|E_{\text{slow}}\rangle$) to a short lifetime at high temperature (where $|E_{\text{fast}}\rangle$ becomes also thermally populated). Martin *et al.*[23] calculated exchange splittings in Si dots assuming a bulklike screened interaction and found the splitting to be much smaller than the observed E_{fast}

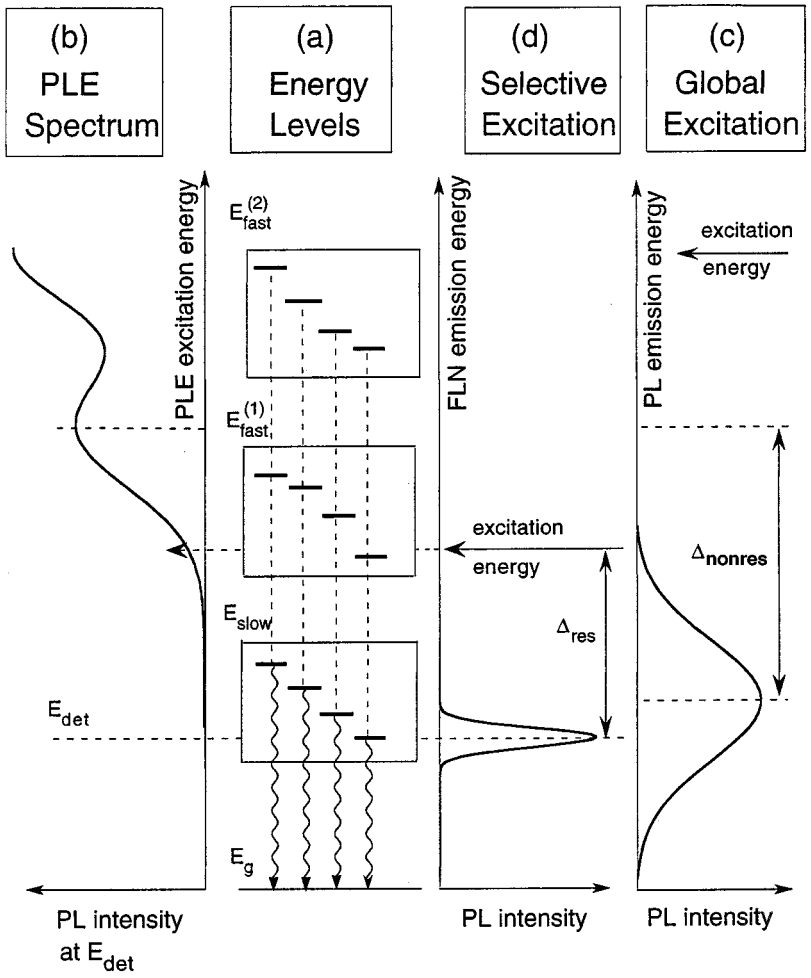

FIG. 1. Schematic diagram illustrating how the basic spectroscopic information in quantum dots is obtained via absorption and emission experiments. (a) The excited energy levels of the dots present in a given sample form groups: the lowest-energy group $|E_{\mathrm{slow}}\rangle$ comprises states that are largely forbidden to the ground state $|g\rangle$ and emit slowly, while the higher-energy group $|E_{\mathrm{fast}}\rangle$ are normal allowed states. In each group there are many states corresponding to dots with different sizes: the larger the dot, the lower its energy level in a group. (b) Photoluminescence excitation (PLE) spectroscopy excites the sample continuously and monitors the emission intensity at a fixed detection energy E_{det}, which is normally taken as the lowest emission energy. The PLE spectrum thus reflects the absorption spectra of the optically allowed states. (c) The ''global excitation spectroscopy'' excites the sample at an energy above the absorption peak (so all sizes present in the sample are excited) and the emission is monitored at all energies. The corresponding ''nonresonant Stokes shift'' Δ_{nonres} is the shift of the emission peak with respect to the lowest absorption peak. Δ_{nonres} reflects, among others, the inhomogeneous broadening. In ''selective excitation spectroscopy'' [also called ''fluorescence line narrowing'' (FLN)], one excites selectively the larger dots in the sample by placing the excitation energy at the low-energy (large-cluster) side of the first PLE peak; the emission is thus narrowed considerably, often showing also phonon side bands. The corresponding ''resonant Stokes shift'' Δ_{res} is the difference between the excitation energy and the peak of the narrow emission. Δ_{res} reflects mostly an intrinsic redshift of a given dot size.

$-E_{\mathrm{slow}}$ energy splitting in selectively excited photoluminescence (PL). However, Takagahara[20] criticized the work of Martin *et al.*,[23] showing that a more accurate description of dielectric screening, using the screening constant $\varepsilon_x \sim 3$, produces an exchange splitting in agreement with experiment. A recent calculation[24] of exchange splitting from accurate *microscopic* wave functions casts doubt, however, on previous estimates[20,23] of the exchange splittings based on envelope-function calculations. A model including exchange splitting was also used recently by Efros *et al.*[13] to explain the spectroscopic results on CdSe dots. In this approach, the four highest ($1s d$-like) hole states (i.e., neglecting split-off band) of a spherical dot are allowed to couple with the two lowest ($1s$-like) electron states to produce eight electron-hole excitonic states. A $\mathbf{k}\cdot\mathbf{p}$ calculation in this subspace, using phenomenological exchange integrals and numerous parameters, shows that the lowest exciton state is spin forbidden (''dark exciton'' $|E_{\mathrm{slow}}\rangle$), while only higher-energy states $|E_{\mathrm{fast}}\rangle$ are allowed (''bright exciton''). Using a number of parameters, this model explained[13] the observed resonant redshift as the splitting between E_{slow} and the lowest E_{fast}, while the nonresonant redshift is explained as the splitting between the center of gravity of *all* dipole-allowed states and E_{slow}. Recent magnetic-field experiments were consistent with this model.[13] A recent calculation by Richard *et al.*[25] showed, however, that the inclusion of six rather than four valence bands in the $\mathbf{k}\cdot\mathbf{p}$ Hamiltonian can produce in CdSe a symmetry forbidden $1pf$ (rather than $1s d$) hole state *even without an exchange interaction*. Thus the $|E_{\mathrm{slow}}\rangle$ to $|g\rangle$ transition could be *spatially* forbidden, not spin forbidden.

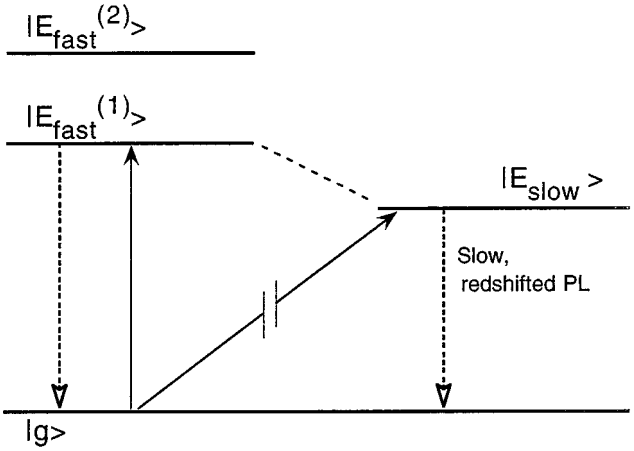

FIG. 2. Schematic illustration of the slow, redshifted PL from state $|E_{\rm slow}\rangle$ relative to the fast PL from state $|E_{\rm fast}^{(1)}\rangle$. The solid arrow is used for the absorption and the dash arrow for the photoluminescence. The broken solid arrow indicates the forbidden transition.

(ii) Intrinsic, orbitally forbidden conduction state. The lowest-energy electron-hole state $|E_{\rm slow}\rangle$ could be dipole forbidden to the ground state $|g\rangle$ if the single-particle electron component of $|E_{\rm slow}\rangle$ is *spatially forbidden* with respect to $|g\rangle$ due to the difference of *Bloch wave functions* for these two states. For example, if the one-electron valence-band maximum (VBM) is a Γ_{15v}-like state, but the one-electron conduction-band minimum (CBM) is an X_{1c}-like state, the zero-phonon single-particle $\Gamma_{15v}\rightarrow X_{1c}$ transition dipole will be zero. Of course, multiband intervalley mixing due to the finite size of dot can relax this strict condition somewhat, leading to a finite transition probability (long radiative lifetime). In general, an X_{1c}-like CBM in a dot can occur as follows: In zinc-blende semiconductors, the effective mass of Γ electrons is lighter than that of X electrons, so as the nanocrystallite becomes smaller, the conduction band at Γ moves upward (due to kinetic-energy confinement) at a greater rate than the conduction band at X. Thus, if the bulk X_{1c} state is not too much higher than the Γ_{1c} state, one expects to find an X_{1c}-like CBM for a sufficiently small quantum dot. This direct-to-indirect crossover was recently predicted to occur for free-standing and for AlAs-embedded GaAs dots, wires, and films.[26] This effect of the $\Gamma\rightarrow X$ CBM crossover as size decreases is not expected to occur in ''strongly direct'' materials where the X_{1c} state is far higher than Γ_{1c} in bulk (e.g., ZnS, ZnSe, and CdSe). In cases where the crossover does occur, there is a natural explanation of the slow-emitting low-energy $|E_{\rm slow}\rangle$ state as being X_{1c}-like.

(iii) Intrinsic, orbitally forbidden valence state. Another scenario for orbitally forbidden transitions is where the *envelope functions* of the electron and hole states have different spatial symmetries. In spherical dots of zinc-blende materials experiencing an infinite potential barrier, the lowest electron state has a $1s$ envelope-function symmetry, while according to a six-band model of Richard *et al.*[25] the highest hole state can be either the symmetry-allowed $1sd$ or the symmetry-forbidden $1pf$. For sufficiently small dots, the $1pf$ state is the highest hole state, so the dipole transition element between this $1pf$ VBM and the $1s$ CBM is zero. This was predicted by Grigoryan *et al.*[27] to be the case for CdS dots with diameter $D<40$ Å and by Richard *et al.*[25] also for CdS dots but at $D<25$ Å (Fig. 3 in Ref. 25) and for InP dots at all sizes (Fig. 5 in Ref. 25). Regrettably, in simplified $\mathbf{k}\cdot\mathbf{p}$ models, the order of the hole states is very sensitive to the (Luttinger) parameters of the models and the level ordering can easily be altered by rather small changes in the empirical parameters. In cases where the envelope function of the hole is $1pf$-like, the $|E_{\rm slow}\rangle\rightarrow|g\rangle$ transition will be both red shifted and slow.

(iv) Extrinsic surface states. Since the surface-to-volume ratio increases rapidly as the dot size decreases, many authors[2–10,14,15] have sought an explanation to carrier dynamics in dots in terms of trapping by *surface states* $|E_{\rm slow}\rangle$. However, a large surface-to-volume ratio implies important surface effects only if the band-edge wave-functions ''feel'' the surface, i.e., have a significant amplitude at the surface. In fact, pseudopotential calculations on passivated Si dots[28] and wires[29] show that the wave functions of band-edge states have very little amplitude at the surface, just as the traditional infinite barrier particle-in-a-box models have always assumed. However, *surface defects*[30] or self-trapped surface excitons[31] could lead to surface states in the fundamental gap (see below). The evidence for the *existence* of surface defect states in dots is reasonably strong, but the evidence for their *roles in carrier dynamics* is not conclusive. For example, evidences for the *existence* of surface states include the detection of dangling bonds in porous Si via electron paramagnetic resonance[2,32,33] and the observation of a unique chemical shift in CdS (Ref. 34) and CdSe (Ref. 35) dots via nuclear magnetic resonance. Recently, x-ray photoemission experiments on colloidal CdSe dots[36] determined that the majority of the Se atoms at the dot surface are uncapped in the as-prepared samples and that the Cd atoms are only partially capped to the ligands because of the steric hindrance of the bulky ligands. Regarding the evidence for the *role* of surface states in carrier dynamics, we note that surface states have been implicated in explaining the slowly emitting state in porous Si,[3–6] including the deep IR emission at $\sim$1 eV with its $\sim$130-meV redshift as well as the yellow-green emission at $\sim$1.8–2.0 eV having a 10 μsec to 1 msec lifetime.[6] Similarly, the long radiative lifetime [$\sim$1 μsec at 10 K (Refs. 7–10, 14, and 15)] and the small quantum yield of the emission[37] in II-VI quantum dots have been explained via surface traps. The emission at 850 nm (1.46 eV) in as-grown colloidal InP dots has also been attributed to a surface state[16] since this state disappears upon HF etching. Bawendi and co-workers[11] have recently revised their earlier view,[7–10] attributing instead the slow, redshifted emission in CdSe to intrinsic spin-forbidden transitions[12,13] [i.e., mechanism (i) above] rather than to extrinsic surface states.

While the existing theoretical works[13,20,25,27,38–42] on the spectra of isolated quantum dots were useful to understand the possible reasons for the redshift, these investigations have some limitations.

(a) Most theoretical approaches assume a surfaceless (i.e., infinite barrier) model, so surface states are excluded from any discussion at the outset. Surfaceless model includes all effective-mass-based approaches,[20] the $\mathbf{k}\cdot\mathbf{p}$ theory,[13,25,39,40] and truncated crystals.[41]

(b) The tradition in the field seems to have been to select one out of at least four possible explanations [(i)–(iv) above]

for the identity of the slow, redshifted emission in particular dots and model it in detail without comparing it to alternative explanations. For example, Efros *et al.*[13] examined for CdSe the effect (i) of an intrinsic, spin-forbidden state; Richard *et al.*[25] examined for a few semiconductor dots the effect (iii) of an intrinsic, orbitally forbidden valence state, while Grigoryan *et al.*[27] examined it for CdS; Garilenko, Vogl, and Koch[42] examined for Si the effect (iv) of surface states and Tsiper[43] offered a ''universal explanation'' that is independent of any feature of the electronic structure of the dots.

(c) Most theoretical approaches employ the parameters that either lack independent verification (e.g., the scaled exchange splitting in Ref. 13) or have a significant range of numerical uncertainty (e.g., the $\mathbf{k}\cdot\mathbf{p}$ parameters in Ref. 25). In many cases, unfortunately, the conclusions appear to be sensitive to the parameter choices.

In this work, we study the possible origins of the lowest, slow-emitting electronic states in InP quantum dots including the possibilities of surface effect and excitonic exchange splitting. We use a computational approach that includes an explicit dot surface. The electronic structure is calculated both for the fully passivated surface as well as for dot surfaces in which a cation surface dangling bond or an anion surface dangling bond is created. We find the following.

(a) The CBM of an InP dot is *not* derived from the X_{1c} state even for small dots, so model (ii) can be excluded for InP.

(b) The symmetry of the envelope function of the VBM is $1sd$-like (unlike what current $\mathbf{k}\cdot\mathbf{p}$ models[25] predict), so model (iii) can be excluded also.

(c) Regarding the surface state model [mechanism (iv)], we find that *passivated dots have no surface states in the gap*. In fact, we predict that over a wide range of different passivation species the band-edge states of the dots will be unchanged.

(d) However, the selective elimination of passivating atoms produces *surface defect states*, a near-conduction surface defect level for an In dangling bond and a near-valence surface defect level for a P dangling bond. Only the cation dangling bond can be implicated in observed redshifts. The energy of the In dangling-bond surface defect has a weak dependence on size, but this state hybridizes with the intrinsic band edges. Furthermore, the dipole matrix element coupling it to the VBM decreases rapidly with the dot size. The surface defect state could explain the rather low quantum yield and the 1.46-eV emission peak[16] that is eliminated upon etching. However, the calculated redshift versus excitation energy due to the surface defect is too large to explain the resonant redshift measured for the HF-etched InP dots.[17]

(e) The exchange splitting was calculated using atomistic wave functions. Its magnitude and scaling with the dot size are consistent with the observed resonant redshift[17] when the screening of exchange is considered. Thus mechanism (i) is an open possibility.

II. METHOD OF CALCULATION

The electronic structure of the dot was obtained by solving the single-particle equation

$$\left\{-\tfrac{1}{2}\nabla^2+\sum_{\mathbf{R}_n}\sum_{\tau_\alpha} v_\alpha(\mathbf{r}-\mathbf{R}_n-\tau_\alpha)\right\}\psi_i=\epsilon_i\psi_i\,, \qquad (1)$$

where $v_\alpha(\mathbf{r}-\mathbf{R}_n-\tau_\alpha)$ is the screened, nonlocal pseudopotential of the atom of type α located at site τ_α in cell $\mathbf{R}_n$ and ϵ_i is the single-particle (orbital) energy. The atomic types α include the dot atoms (In and P) as well as the passivating, hydrogenlike atoms attached to the surface atoms. Note that Eq. (1) includes an atomistic (not continuum) description of the dot electronic structure and thus effective-mass or $\mathbf{k}\cdot\mathbf{p}$ approximations are avoided.

The screened nonlocal atomic pseudopotentials $\{v_\alpha\}$ are obtained[44,45] in a two-step process. *First*, we invert the self-consistently calculated [via the local-density approximation (LDA)] screened *crystalline* potential of a number of InP structures (zinc-blende, rocksalt, and β-Sn) to find the ''spherical LDA'' potential that reproduces LDA energies and wave functions extremely well. *Then*, we make small adjustments to this potential so as to fit the bulk band structures to the experimentally measured bulk interband-transition energies, while preserving a large ($>99\%$) overlap of the wave functions with the original LDA values. These semiempirical pseudopotentials thus combine LDA-quality wave functions (unlike the conventional ''empirical pseudopotential method''[41,46]) with experimentally consistent excitation energies, effective masses, and deformation potentials (unlike the LDA). These pseudopotentials are deposited in a FTP site[47] and are available for use. Further details of the method to generate these pseudopotentials are provided in Ref. 45. Note that, since in our semiempirical pseudopotential method (SEPM) calculation the average potential [i.e., the $\mathbf{G}=0$ term of the Fourier transform $v_\alpha(\mathbf{G})$ of the potential in Eq. (1)] is explicitly included, all the energy levels obtained are ''absolute'' values in the sense that they have the same reference (i.e., the vacuum potential). We will thus plot individual energy levels (e.g., the VBM and CBM) versus dot size.

The wave functions ψ_i are expanded in a set of plane waves

$$\psi_i(\mathbf{r})=\sum_{\mathbf{G}} A_i(\mathbf{G})e^{i\mathbf{G}\cdot\mathbf{r}}, \qquad (2)$$

where $\mathbf{G}$ are the reciprocal lattice vectors. Each dot is placed in a fictitious ''supercell'' consisting of 6.4 Å of vacuum surrounding the dot. The supercells are repeated periodically so that Eq. (1) can be solved using band-structure techniques. The plane waves in Eq. (2) span both the dot and the vacuum region around it, so that the dot wave functions are not required to vanish exactly at the surface, but can decay smoothly into the vacuum region. The kinetic-energy cutoff of plane-wave bases for the dot is the same as what used to generate the semiempirical pseudopotentials. The matrix elements of $v_\alpha(r)$ within the basis (2) are calculated via accurate numerical Fourier transforms.

We consider four InP dots with different sizes: $(\mathrm{InP})_{107}$, $(\mathrm{InP})_{259}$, $(\mathrm{InP})_{712}$, and $(\mathrm{InP})_{3187}$. The dots have cubic shape with the faces oriented along zinc-blende InP (110), (110), and (001) directions. The dot-interior atomic positions are taken to be bulklike. The surface atomic positions, including those of the passivating atoms, are

TABLE I. Experimental and theoretical excitonic band gaps for InP dots of different sizes. The Coulomb corrections included in the calculated excitonic gaps are given separately.

Dot diameter (Å)	Measured gap (eV)[a]	Calculated gap (eV)	Calculated Coulomb correction (eV)
13.83		2.95	−0.30
18.57		2.52	−0.22
20	2.53		
26	2.38		
26.01		2.12	−0.16
30	2.10		
35	2.04		
38	1.96		
40	1.87		
42.87		1.78	−0.09
44	1.89		
50	1.77		
54	1.68		

[a]Reference 16.

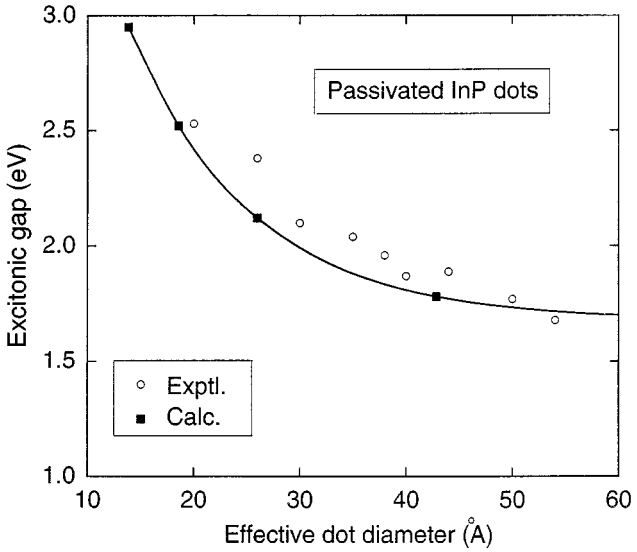

FIG. 3. Calculated excitonic gaps for InP quantum dots with different sizes. The experimentally measured values (Ref. 16) are also included in this figure for comparison. See Table I for numerical values.

obtained[45] by fitting the surface density states of the *flat*, chemically passivated InP surfaces (without reconstruction) to the photoluminescence data.[48] Assuming the same atomic density as in the bulk, the effective dot diameters are given by[49] $d=(a/2)N^{1/3}$, where a is the lattice constant of bulk InP (5.83 Å) and N is number of atoms in the dots. This gives the effective sizes of 13.83, 18.57, 26.01, and 42.87 Å for the above four dots. The numbers of plane-wave basis functions used in calculation are 31 287, 52 519, 102 733, and 315 969, respectively.

Such huge Hamiltonian matrices cannot be solved by ordinary diagonalization methods. We use instead the ''fold spectrum method''[28] in which $H\psi=\epsilon\psi$ [i.e., Eq. (1)] is replaced by $(H-\epsilon_{\rm ref})^2\psi=(\epsilon-\epsilon_{\rm ref})^2\psi$ and $\epsilon_{\rm ref}$ is an arbitrary energy ''pointer.'' Since the lowest eigenvalue of the folded spectrum is now the one closest to $\epsilon_{\rm ref}$ in the latter equation, we can obtain selectively the near-edge eigensolutions by placing the pointer near the VBM or CBM. We thus avoid the computations needed to find *all* the eigensolutions, so the effort involved in the present solution scales linearly with the number of atoms. Further details of the method and the use of the conjugate-gradient approach to solve the pertinent equations are given in Ref. 50.

Our method avoids the restricted variational flexibility of tight-binding approaches.[38,51] Unlike the $\mathbf{k}\cdot\mathbf{p}$ based methods,[13,25,39,40] our approach includes a physical surface, permits coupling of a large number of host crystal bands, and circumvents the effective-mass parabolic band approximation. This method has been applied previously to Si nanostructures,[28,50] to CdSe dots,[52] and to dots, wires, and films of GaAs.[26]

III. RESULTS AND DISCUSSIONS

A. Electronic structures of fully passivated dots

Table I and Fig. 3 show our calculated excitonic band gaps of the *fully passivated* InP dots as a function of dot size, compared with the absorption and photoluminescence data that were obtained for well-passivated dots.[16] We have corrected the calculated single-particle band gap by the electron-hole Coulomb energy using the formula of Ref. 53. It can be seen from Fig. 3 that the agreement between the theoretical calculations and experiments is good.

Figure 4 shows the wave-function squares (averaged along the [001] direction) of the near-edge states of the fully passivated $(InP)_{712}$ dot (effective diameter $d=26.01$ Å). We see that these states can be characterized as ''dot-interior states'' in that their wave functions are distributed mostly in the interior of the dot rather than at the surfaces. This agrees with previous results on Si dots,[28] wires, and films.[29] Thus *there are no surface states in the band gap of fully passivated InP dots*. In fact, the band-edge states remain dot-interior-like over a considerable range of passivating pseudopotentials. Thus we predict that the band-edge states will be rather insensitive to the identity of the passivating species (unless they are extremely electronegative, e.g., oxygen, in which case the band edges could be pinned by the passivant).

The top portion of Table II shows the squared dipole matrix elements calculated for optical transitions between the VBM and the CBM in two fully passivated InP dots. We have normalized the values to the VBM to CBM transition dipole in *bulk* InP with an equivalent number of atoms. Note that the radiative lifetime is inversely proportional to this squared matrix element: The larger the dipole element, the ''more allowed'' the transition and the shorter its radiative lifetime. We see that the near-edge transitions in passivated InP dots are strongly allowed. Examination of the CBM wave functions via projection onto bulk wave functions further shows that the dot CBM is mostly derived from the *direct* Γ_{1c} band-edge state, not from the indirect X_{1c} state, which is the case in small GaAs dots.[26] We can thus *exclude* (see the Introduction) mechanism (ii) (intrinsic, orbitally forbidden conduction state) and mechanism (iii) (intrinsic, orbitally forbidden valence state[25,27]) as being inappropriate to InP. The reason why a direct (Γ_{1c}) to indirect (X_{1c}) cross-

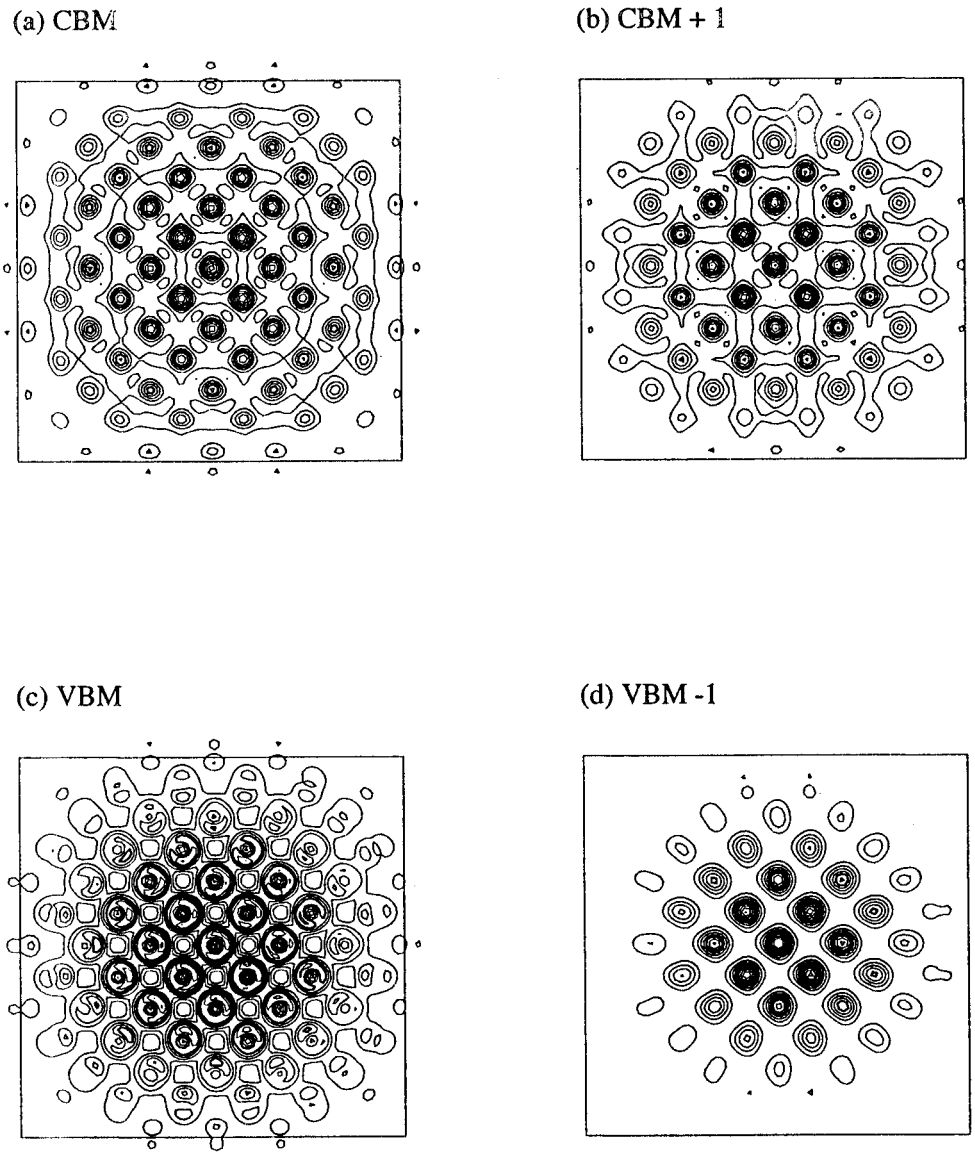

FIG. 4. Contour plots of the wave-function squares of the CBM (the lowest conduction state), CBM+1 (the next lowest conduction state), VBM (the double-degenerate highest valence state), and VBM-1 (the next highest valence state) of a fully passivated $(InP)_{712}$ dot with size $d=26.01$ Å. The plotted wave-function squares are averaged along the (001) direction. The *frame* in each plot denotes the dot boundary where the outermost surface In or P atoms are located. Note that none of these states are surfacelike.

over does not occur in InP dots is the existence of a large $X_{1c}-\Gamma_{1c}$ energy difference in *bulk* InP (0.85 eV in InP compared with 0.48 eV in bulk GaAs). The reason that the VBM of the InP dot in our calculation is not the dipole-forbidden $1pf$ state predicted by Richard *et al.*[25] is probably related to the simplified assumptions made in the latter calculation: perfect spherical symmetry, an infinite potential barrier, no surface, and a limited range of interband coupling.

B. Exchange splitting in fully passivated dots

The electron-hole correlation in small quantum dot is negligible.[54] The exchange splitting between excitonic singlet and triplet states can be calculated in the framework of the definition of the exact exchange[55]

$$E_{\text{exch}}=2e^2\int \frac{\psi_e^*(\mathbf{r}_e)\psi_h^*(\mathbf{r}_h)\psi_h(\mathbf{r}_e)\psi_e(\mathbf{r}_h)}{\varepsilon(|\mathbf{r}_e-\mathbf{r}_h|)|\mathbf{r}_e-\mathbf{r}_h|}\,d\mathbf{r}_e d\mathbf{r}_h, \quad (3)$$

TABLE II. Momentum matrix element squares $|\langle i|\hat{p}|f\rangle|^2$ between the initial state $|i\rangle$ and the final state $|f\rangle$. The calculated values are normalized to the direct $\Gamma_{15v}\rightarrow\Gamma_{1c}$ transition probability in bulk InP.

Relative dipole matrix elements	Dot diameter $D=13.83$ Å	Dot diameter $D=26.01$ Å
Fully passivated dot		
M^2(VBM to CBM)/M^2_{bulk}	0.4001	0.5263
Dots with an In DB		
M^2(VBM to In DB)/M^2_{bulk}	0.0832	0.0272
M^2(VBM to CBM)/M^2_{bulk}	0.3387	0.4995
Dots with a P DB		
M^2(P DB to CBM)/M^2_{bulk}	0.0282	0.0143
M^2(VBM to CBM)/M^2_{bulk}	0.2422	0.4537

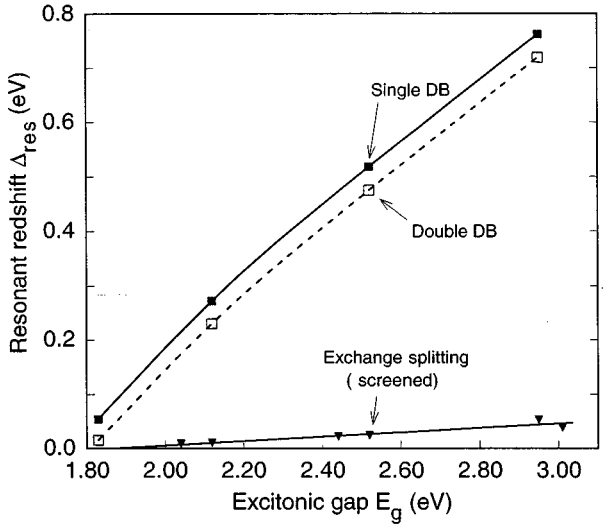

FIG. 5. Calculated resonant redshift in InP quantum dots versus the excitonic gaps, showing (a) the redshifts due to the surface-state mechanism (including a single In dangling bond and interacting dangling bonds) and (b) the redshift due to exchange splittings calculated with the distance-dependent Thomas-Fermi dielectric screening constant. The lines in this figure are a guide for eyes.

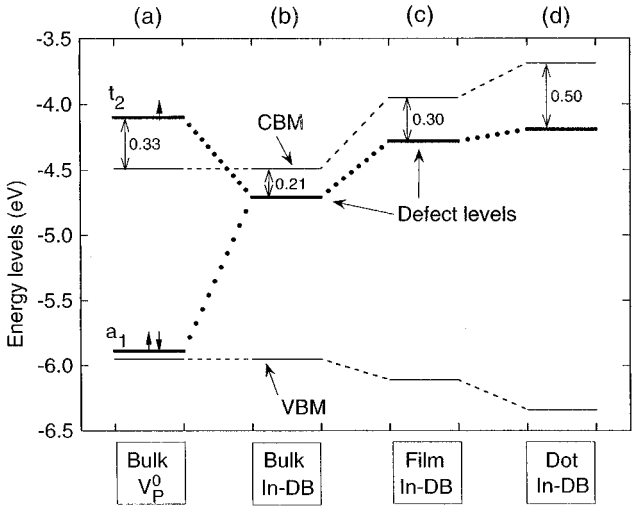

FIG. 6. Energy levels for different In dangling-bond defects: (a) a neutral P vacancy in bulk InP, giving rise to four In dangling bonds; (b) a single In dangling bond in bulk; (c) a single In dangling bond at the 9-ML InP(110) film; and (d) a single In dangling bond at the surface of the $d=18.57$ Å dot.

where ψ_e and ψ_h are, respectively, the electron and hole single-particle wave functions and are obtained from our direct pseudopotential calculation of Eq. (1). Here the distance-dependent Thomas-Fermi dielectric function[56] is used to describe the screening of the exchange interaction, i.e.,

$$\varepsilon(r)=\begin{cases}\varepsilon(0,d)\,\dfrac{qR}{\sinh[q(R-r)]+qr}, & r\leq R\\ \varepsilon(0,d), & r>R\end{cases} \tag{4}$$

where $q^2=4(3\pi^2 n_0)^{1/3}/\pi$ (n_0 is the average density of the valence electrons at the equilibrium volume) and R is the screening length determined by

$$\sinh(qR)/qR=\varepsilon(0,d). \tag{5}$$

Note that for large r, the function $\varepsilon(r)$ approaches the value $\varepsilon(0,d)$. The static dielectric constant $\varepsilon(0,d)$ in the quantum dot is different from the bulk value[57] and depends on the dot size d. We use for $\varepsilon(0,d)$ the modified Penn model,[57,58] i.e., $\varepsilon(0,d)=1.0+11.4/[1.0+(12.094/d)^2]$ (the size d is in units of angstroms).

Our calculated exchange splittings for cubic dots with effective diameters of 13.81, 18.57, and 26.01 Å are 52.9, 24.1, and 10.4 meV, respectively. We also calculate the exchange splittings for some spherical dots and obtain the exchange values of 37.9, 22.0, and 8.8 meV for dot sizes 16.02, 23.68, and 34.79 Å, respectively. This shows that the exchange splittings in dots are substantially enhanced compared with the bulk ($\sim$1 meV). The calculated exchange splittings for different dot sizes are plotted in Fig. 5 as a function of the excitonic gap. The relationship is seen to be nearly linear.

The fact that screening the exchange by $\varepsilon(r)$ [Eq. (4)] affects significantly the numerical value of the exchange shows that at large-r values the exchange interactions are not negligible. Thus, contrary to previous assumptions, our calculation supports the view that exchange interactions in dots are not short ranged.

C. Electronic structure of dots with model surface dangling bond

Given that fully passivated dots have no surface states, we now remove deliberately passivating atom so as to expose surface dangling bonds. The calculation described in what follows is a model calculation, in that we do not know the actual, potentially complex structure of the real surface of a colloidal dot. Generally, such a surface could include many interacting dangling bonds, ''weak'' surface bonds, partially reconstructed surface patches, and various surface-ligand bonding configurations. Our approach is to first model the surface of the *fully passivated* dots after the experimental results of flat, passivated InP surfaces[48] (in which reconstruction is removed via chemisorption) and then create an isolated In dangling bond (DB) and separately an isolated P dangling bond to study their generic effects on the electronic structure of the quantum dot. Such isolated dangling bonds represent, most likely, a stronger perturbation than what would be expected to occur in a real surface, having interacting and partially rebonded dangling bonds.

We position the In and P dangling bonds near the center of the dot surface formed on the (110) plane. Dangling bonds at other sites were also studied. Due to the highly localized nature of the dangling-bond wave functions, we found only slight difference (less than 0.15 eV) in the energy levels, depending on the precise position of the dangling bond.

1. The indium dangling bond at the dot surface

Figure 6 shows the relative energy position of an In dangling-bond state in a small dot ($d=18.38$ Å), clarifying how this state evolves from the bulk vacancy states. Creation of a neutral P vacancy (V_P^0) in bulk InP produces four In dangling bonds, giving rise to a doubly occupied singly de-

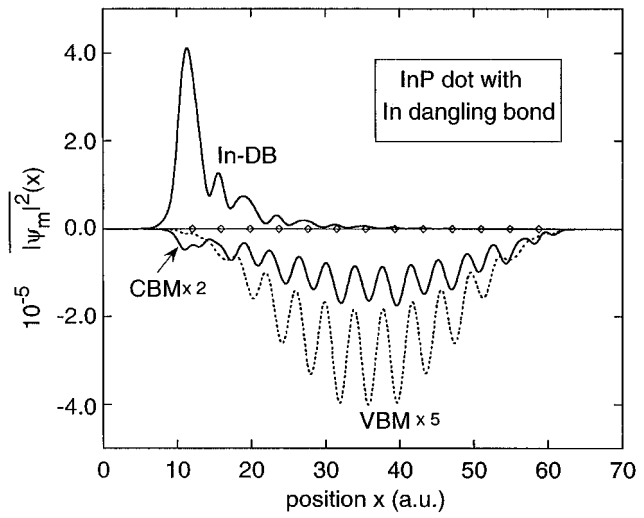

FIG. 7. Planar-averaged wave-function squares of the In DB surface state, the CBM, and the VBM states for the $(InP)_{712}$ dot with an In dangling bond. The positions of the atomic layer along the plotted (110) direction are indicated by the empty diamond symbols at the horizontal axis. Note the localization nature of the In DB state and the dot-interior nature of the CBM and VBM.

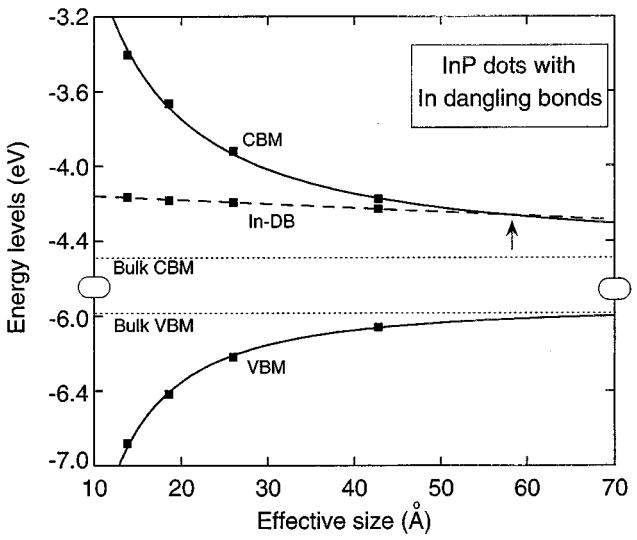

FIG. 8. Variations of the In DB surface state, the CBM, and the VBM states with the dot size for InP dots with an In dangling bond. The arrow indicates the dot size where the lowest unoccupied state changes from surfacelike to dot-interior-like.

generate a_1 state near the VBM and a singly occupied triply degenerate t_2 state above the CBM [Fig. 6(a)].[59–63] The interaction between these four dangling bonds spreads their energies: The energy difference between the a_1 state and the *isolated* DB energy is three times the difference between t_2 state and the isolated DB energy.[64] To create a *single* isolated DB, we then passivate three of the four bulk DB's. The a_1 and t_2 levels of the bulk vacancy then give rise to a single bulk In DB state near the CBM [Fig. 6(b)]. As we bring this DB from the interior of the three-dimensional (3D) bulk to the surface of a 2D film [Fig. 6(c)], the DB state partially tracks the film's CBM, which rises in energy due to quantum confinement. Similarly, as one progresses from a 2D film to a 0D dot, the CBM rises further and with it the In dangling-bond level. We thus see from the study of Fig. 6 that the In dangling-bond state in an InP dot is generically similar to the analogous dangling-bond state in the bulk (but not to the bulk vacancy, which consists of four, strongly interacting dangling bonds). However, as we will see below, the relative energy position (and thus the interaction and wave-function mixing) of the CBM and the DB state in quantum dots can be changed as the dot size is altered.

Figure 7 depicts the planar-averaged wave-function squares of the near-edge states for the 26.01-Å dot with an In dangling bond. It shows that both the VBM and the CBM are delocalized in the interior of dot, while the In DB state is strongly localized at the surface site where an In DB is created.

Figure 8 shows as a function of dot size the orbital energies of the In dangling-bond state, the extended CBM state, and the VBM state. It can be seen that, unlike the dot-interior state CBM and the VBM, the surface-localized In DB state changes very little (less than 20 meV) as the dot size changes. The In DB state is the lowest unoccupied level for dots with diameter up to 57 Å, at which point the dot-interior, extended conduction CBM state becomes the lowest unoccupied state. Thus the lowest unoccupied state changes from surfacelike (In DB) to bulklike (CBM) at a critical size (the value of this critical size may change slightly depending on the location of dangling bond, but the *existence* of crossing is reasonably certain).

We have seen that in the fully passivated dots (Sec. III A) the band-edge states do not depend much on the identity of the passivating atom. In a similar way, the energy and wave function of the surface defect level (e.g., In DB) do not depend much on the identity of the passivating atom, since the surface defect is an *intrinsic* defect, made up of In and P orbitals, not from those of the passivating atoms. We thus expect that, as long as there are some dangling bonds in a dot, the dangling-bond spectrum will be largely unchanged as one alters the (incomplete) passivation.

Table II shows the dipole transition moments between the valence-band maximum and the two lowest unoccupied states in InP dots with In DB's. We see that the VBM to In DB transition has a 4–18 times lower oscillator strength (thus a longer radiative lifetime) than the transition from the VBM to the extended, dot-interior conduction CBM state. Furthermore, the probability of the VBM to In DB transition decreases with the increasing dot size, while that of the VBM to the CBM transition increases. Thus the larger the dot, the longer the radiative lifetime of the VBM to In DB transition.

The presence of In dangling bond in a quantum dot shifts the dot CBM up relative to the CBM of a *fully* passivated dot, while the dot VBM does not change much ($\leqslant 0.5$ meV). These shifts of the CBM's are given in the second column of Table III and are seen to decrease with the increasing dot size.

2. The phosphorus dangling bond at the dot surface

Figure 9 shows how the phosphorus dangling-bond state in an InP dot [Fig. 9(d)] develops from the bulk In vacancy V_{In}^0. An In vacancy creates a singly degenerate and doubly occupied a_1 state deep inside the valence band and a triply occupied triply degenerate t_2 state at $\epsilon_{VBM}+0.39$ eV [Fig. 9(a)].[65] When three of the four P DB's are passivated, the

TABLE III. Upward shift of the CBM (VBM) of ideally passivated dots due to the introduction of In (P) dangling bond. All energies in this table are in units of meV.

Dot diameter (Å)	CBM shift (for In DB)	VBM shift (for P DB)
13.83	28.9	249.5
18.57	17.3	74.5
26.01	12.1	20.3

a_1 and t_2 levels give rise to a single DB state just above the VBM [Fig. 9(b)]. This level is nearly constant in energy at the InP(110) film [Fig. 9(c)] and at the surface of dot [Fig. 9(d)], except that the VBM energies are lowered due to quantum confinement. Analyses of the P DB defect-level wave functions show that they are more localized than the In DB wave functions. Additionally, unlike the sp-hybrid nature of In DB wave functions, the P DB wave functions are pure p-like. Figure 10 shows the planar-averaged wave-function squares of the near-edge states of an $(InP)_{712}$ dot with P DB. The P DB state is highly localized at the dot surface, while the VBM and CBM states are extended in the interior of the dot.

Figure 11 shows the energy dependences of the P DB state, the VBM state, and the CBM state on the dot size. Owing to the extreme localization of its wave function, the energy of the P DB state is almost independent of the dot size. However, as Table III shows, the presence of a P dangling bond shifts the dot VBM upward relative to the VBM of the fully passivated dot [by as much as 250 meV for $(InP)_{107}$], while the dot CBM does not change much. Table III also shows that the shift of the dot VBM due to the P dangling bond is much larger than the shift of the dot CBM due to the In dangling bond, especially for small dots.

Table II shows the dipole matrix elements of the localized-to-extended P DB to CBM transition, indicating

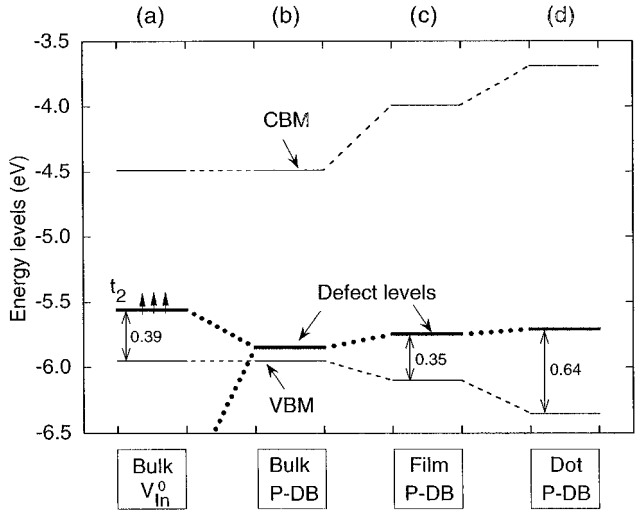

FIG. 9. Energy levels for different P dangling-bond defects: (a) neutral In vacancy in bulk InP, giving rise to four P dangling bonds; (b) a single P dangling bond in the bulk; (c) a single P dangling bond at the InP(110) film with 9 ML thickness; and (d) a single P dangling bond at the surface of the $d=18.57$ Å dot.

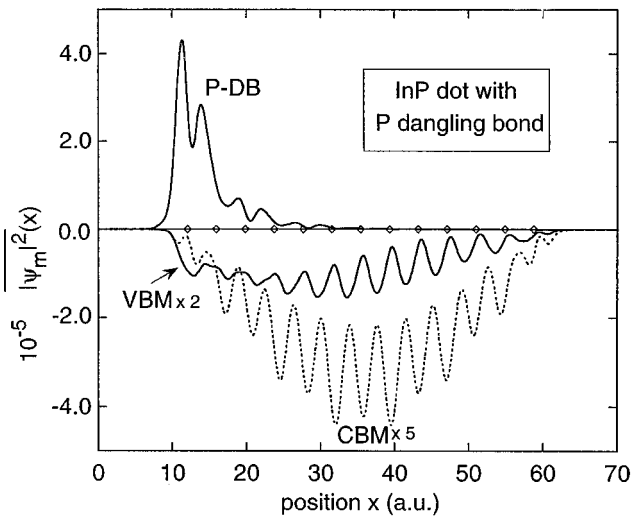

FIG. 10. Planar-averaged wave-function squares of the P DB surface state, the CBM, and the VBM states for the $(InP)_{712}$ dot with a P dangling bond. The positions of atomic layer are indicated by the empty diamond symbols at the horizontal axis.

that this is a weak transition with a long radiative lifetime, while the extended-to-extended VBM to CBM transition is much stronger and has a shorter radiative lifetime. The P DB state, being just above the valence band (see Fig. 11), can act as a trap to photogenerated holes from the valence band. Thus, if P DB's exist, they will trap holes and lead to long hole lifetimes. In practice, owing to the chemical reactivity of a P DB site, it is likely to have but a small concentration.[16]

D. Discussion of surface dangling bonds and exchange effects

We have seen that our theory excludes two possible mechanisms for the red-shifted, slow emissions in InP dots, namely, $|E_{\text{slow}}\rangle$ cannot be due to (ii) an intrinsic, orbitally forbidden conduction state or (iii) an intrinsic, orbitally forbidden valence state. Also, the near-valence-band P DB surface state is not a likely candidate to explain a near-conduction-band shift observed experimentally. We are left

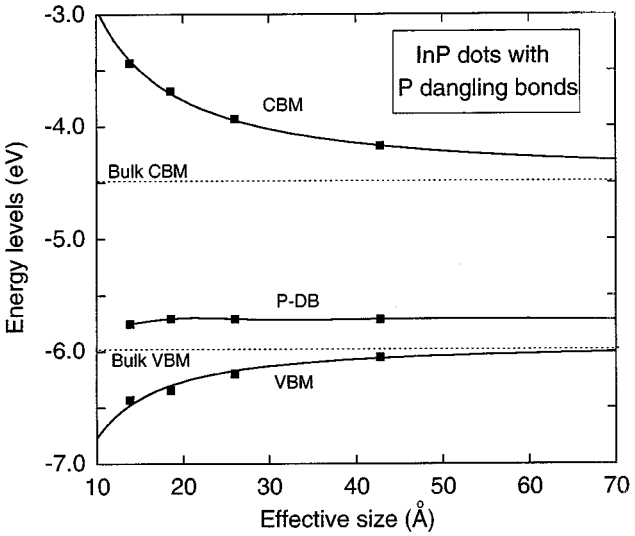

FIG. 11. Variations of the P DB surface state, the CBM, and the CBM states with the dot size for InP dots with a P dangling bond.

with two possibilities, i.e., the In surface dangling-bond state and the exchange splitting mechanism.

1. Global excitation experiments and the In DB state

Our theoretical results on the In DB surface defect can be compared with experimental *global excitation measurements*,[16] in which different chemical etchants and passivants [tri-*n*-octylphosphine oxide (TOPO) and HF] were used to etch and passivate the InP quantum dots. Two types of global PL peaks were observed: a short lifetime (5–50 nsec at $T=300$ K) peak, which does not change its energy for different surface passivants, suggesting that it originates from an intrinsic, dot-interior state; and a long-lifetime (500 nsec at $T=300$ K) PL peak, which dramatically reduces its intensity when the dot is passivated by HF, suggesting that it could originate from a dot surface state. Both types of PL peaks are red shifted relative to the absorption peak.

The redshift of the intrinsic, short-lifetime global PL peak is quite large,[16,17] being 180 meV for an average size of 30 Å. As shown schematically in Fig. 1(c), this nonresonant redshift arises because one excites *more than one* inhomogeneously broadened electronic state (e.g., $E_{\rm fast}^{(1)}$ and $E_{\rm fast}^{(2)}$) as compared to a single inhomogeneously broadened state in selective excitation [Fig. 1(d)].

The redshift of the long-lifetime PL peak could be due to surface defect for three reasons. (a) The peak is removed by HF surface etching. (b) The long-lifetime PL peak is measured[16] ~ 350 meV below the dot-interior related PL peak for the dot with $d\approx 30$ Å. Our calculation shows that for dot sizes less than 57 Å, the In DB state is below the dot-interior CBM state (Fig. 8). For the $d=26$ Å dot, the In DB surface state is predicted to lie 300 meV below the dot-interior CBM state, in good agreement with the experimental value. (c) The measured ratio[16] of the lifetime of the surface-related PL peak to that of the dot-interior peak is 10–100 for $d\approx 30$ Å. Our calculation (Table II) for the nearest size $d=26$ Å shows that the lifetime ratio of the VBM to In DB transition to the VBM to CBM transition is 18. Our calculation also shows that this lifetime ratio increases with increasing dot size.

The results of Fig. 8 and Table II then suggest that the In DB state is a possible origin of the low-energy, slowly emitting state $|E_{\rm slow}\rangle$ (Fig. 2) observed[16] in global excitation [Fig. 1(c)] prior to HF etching of the dot. The strong absorption will occur from the VBM to the CBM, following an intersystem crossing to the In DB state, which is the slowly emitting state for dots smaller than 57 Å. The surface-state-induced redshift will vanish for dots larger than 57 Å, where the lowest unoccupied state becomes the dot-interior CBM state. The redshift $E_{\rm CBM}-E_{\rm In\,DB}$ is plotted in Fig. 5 with respect to the excitonic gap (which is close to $E_{\rm CBM}-E_{\rm VBM}$), showing a nearly linear dependence.[66]

Bawendi and co-workers[11] found that the red-shifted FLN emission spectrum of CdSe dots closely resembles the absorption spectrum (as measured by pump-probe experiment). Since in a surface state model the absorption and emission will presumably commence from spatially *different* electronic states (''corelike'' and ''surfacelike''), the spectral resemblance of absorption and emission suggested to them that some intrinsic states are involved rather than surface states. This is not a compelling argument since the surface dangling-bond state and the dot-interior conduction state are electronically coupled so their spectral properties could very well resemble each other.

2. Selective excitation experiments and the singlet-triplet states

While the 350-meV redshift observed in *global excitation experiments*[16] prior to etching can be tentatively explained by the surface-defect mechanism, as we will see below, the redshift seen in *selective excitation* [Fig. 1(d)] for HF-etched and passivated InP dots[17] cannot. Before comparing theory and experiment, however, we need to analyze the experimental FLN data[17] to extract from it the quantity that is comparable with theory. Conventional samples include dots of many sizes $\{d\}$, with a typical size distribution[67]

$$P(d,\langle d\rangle)=\frac{1}{\sqrt{2\pi}\sigma_d}\,e^{-(d-\langle d\rangle)^2/2\sigma_d^2}, \tag{6}$$

with the average size $\langle d\rangle$. The standard deviation σ_d can be deduced from transmission electron microscopy (TEM).[16] Because of the existence of a size distribution of dots, each emitting at its own characteristic energy, the measured emission line shape represents an ensemble average, denoted here as $\overline{I_{\rm PL}}(\varepsilon,\varepsilon_{\rm excit},\langle d\rangle)$, where $\varepsilon_{\rm excit}$ is the excitation energy. It is of interest to extract from the measured $\overline{I_{\rm PL}}(\varepsilon,\varepsilon_{\rm excit},\langle d\rangle)$ versus $\varepsilon_{\rm excit}$ the underlying single-dot redshift for two reasons: (i) Theory calculates single-dot quantities, not the ensemble average, and (ii) part of the observed ensemble redshift is due to the size distribution effect, not an intrinsic effect, and it is necessary to separate these contributions.

To extract the single-dot redshift from the measured FLN, we simulate the ensemble emission intensity as

$$\overline{I_{\rm PL}}(\varepsilon,\varepsilon_{\rm excit},\langle d\rangle)=\sum_{d>d_c(\varepsilon_{\rm excit})}\alpha(\varepsilon_{\rm excit},d)I_{\rm PL}(\varepsilon,d)P(d,\langle d\rangle). \tag{7}$$

Here $\alpha(\varepsilon_{\rm excit},d)$ is the single-dot absorption coefficient at the energy $\varepsilon_{\rm excit}$ and $I_{\rm PL}(\varepsilon,d)$ is the single-dot emission intensity. We assume that each dot absorbs at the energy $\varepsilon_{\rm excit}\geqslant E_g(d)$ of its excitonic band gap and emits at $E_g(d)-\Delta(d)$, where $\Delta(d)$ is the single-dot redshift that we wish to determine. The single-dot emission intensity is taken as

$$I_{\rm PL}(\varepsilon,d)=\frac{1}{\sqrt{2\pi}\sigma_{\rm PL}}\,e^{-\{\varepsilon-[E_g(d)-\Delta(d)]\}^2/2\sigma_{\rm PL}^2}, \tag{8}$$

where $\sigma_{\rm PL}$ is the intrinsic broadening of the emission of a single dot, interacting in the ensemble with all other dots. The excitonic gap of a single dot is

$$E_g(d)=E_g(\infty)+\frac{A}{d^n}, \tag{9}$$

where $E_g(\infty)$ is the bulk band gap (1.45 eV for InP at $T=10$ K). For passivated InP dots, $E_g(d)$ of Fig. 3 can be well described by $A=55.2527$ and $n=1.3611$ (E_g and d are in units of eV and Å, respectively). The single-dot redshift is taken in the form

$$\Delta(d)=B/d^m, \tag{10}$$

where B and m are to be determined by fitting the measurements. The sum over d in Eq. (7) is limited to those values satisfying $E_g(d) \leqslant \varepsilon_{\text{excit}}$.

We fitted the data of Micic *et al.*[17] for $\langle d \rangle = 32$ Å, using $\sigma_d = 2.5$ Å (the average of the TEM measured values of Ref. 16) and $\sigma_{\text{PL}} = 2$ meV and taking $\alpha(\varepsilon, d)$ to be a constant over the small range of excitation energies involved. Denoting the energy of the peak of the ensemble emission $I_{\text{PL}}(\varepsilon, \varepsilon_{\text{excit}}, \langle d \rangle)$ as $\varepsilon_{\text{peak}}(\varepsilon_{\text{excit}}, \langle d \rangle)$, we define the ensemble redshift as

$$\tilde{\Delta}(\varepsilon_{\text{excit}}, \langle d \rangle) \equiv \varepsilon_{\text{excit}} - \varepsilon_{\text{peak}}(\varepsilon_{\text{excit}}, \langle d \rangle). \tag{11}$$

Here only the main conclusions about the single-dot redshift are discussed, while the detail of the simulation results will be given in Ref. 17. In the simulation, the best fit occurs at

$$\Delta_{\text{expt}}(d) = 9500/d^{1.96} \ \text{(meV)}. \tag{12}$$

While the fit is sensitive to the assumed σ_{PL} value, the range of σ_{PL} can be narrowed down significantly by requiring that the simulated half-width of $I_{\text{PL}}(\varepsilon, \varepsilon_{\text{excit}}, \langle d \rangle)$ match experiment. This is satisfied at $\sigma_{\text{PL}} \simeq 2-4$ meV.

We find that the single-dot redshift $\Delta_{\text{expt}}(\varepsilon_{\text{excit}})$ is considerably smaller than the ensemble redshift $\tilde{\Delta}(\varepsilon_{\text{excit}})$ and has a different slope. Furthermore, even if we assume in Eq. (7) that $\Delta(d) \equiv 0$, we still find that $\tilde{\Delta} \neq 0$. Thus a part of the observed ensemble redshift comes only from the existence of a size distribution, not from an intrinsic effect.

Our results show that the magnitude of the observed single-dot redshift $\Delta(\varepsilon_{\text{excit}})$ is far smaller than the values predicted for the In DB surface defect. For example, at the excitation energy of 2.0 eV (corresponding to a dot size 36 Å in experiment), the observed $\Delta(\varepsilon_{\text{excit}})$ is 8 meV [Eq. (12)], while the calculated single DB redshift is 180 meV (Fig. 5). We have also calculated the surface-state-induced redshift for dots with *two* nearest-neighbor dangling bonds (dash line in Fig. 5) and find that the interaction between these DB's does not change much the slope of the redshift versus gap curve.[68] Thus simple In dangling bonds are insufficient to explain the resonant redshift.[17] It is possible that more complicated surface chemistry (including oxygen atoms) could explain the observed resonant redshift, but we can exclude *simple* dangling bonds as an explanation for the resonant redshift.

Figure 12 depicts the single-dot redshift $\Delta_{\text{expt}}(d)$ deduced from fitting the measured FLN data in comparison with the calculated screened exchange splittings (Sec. III B). Figure 12 shows that the screened exchange splittings agree quite well with experiment. It suggests that the observed *resonant* redshift could originate from the excitonic exchange splitting. It will be interesting to measure the lifetime versus size since in the excitonic exchange model one expects but a weak dependence of lifetime on size, while the surface state model suggests longer lifetimes for larger dots (Table II).

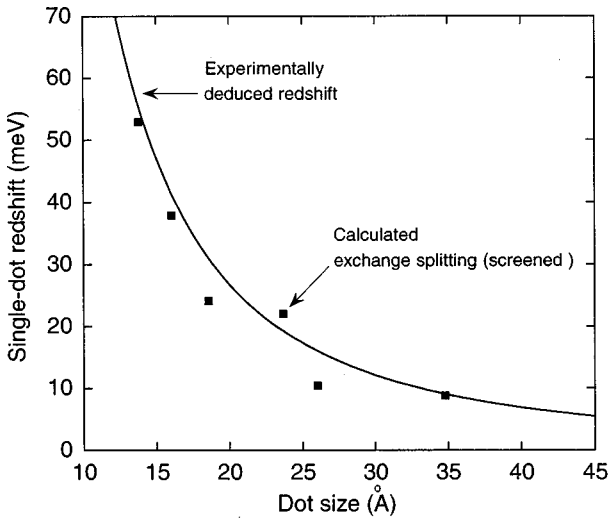

FIG. 12. Single-dot redshifts $\Delta(d)$ from the simulation [Eq. (12)] and the calculated screened exchange splittings [Eq. (3)] for different dot sizes.

IV. SUMMARY

We have performed an *atomistic* electronic-structure calculation on InP quantum dots, avoiding simple approximations used previously,[13,25,39,41] e.g., the use of infinite potential barriers, the neglect of the dot surface, the restriction of the interband coupling to only the VBM and CBM derived states, the use of effective-mass-based approaches, and the phenomenological modeling of the exchange interactions. Our main findings are as follows.

(i) The calculated excitonic gap versus dot size of InP [as well as CdSe (Ref. 52)] is in good accord with measurements; the scaling of the InP excitonic gap with size is $d^{-1.36}$. The scaling of the single-particle band gap with size is[45] $d^{-1.16}$; the simple effective-mass theory predicts d^{-2}.

(ii) A fully passivated dot has no surface states, even down to small dot sizes (the same is true for[29] Si). This situation remains for a broad range of passivating atoms (except, perhaps, oxygen).

(iii) The lowest unoccupied state of a fully passivated InP dot evolves mostly from the Γ_{1c} state of the bulk crystal band down to small dot sizes. This is unlike the case in GaAs dots, where at small dot sizes the lowest unoccupied state is predicted[26] to become the indirect, X_{1c}-like band-edge state.

(iv) The highest occupied state of the fully passivated dot has a $1sd$ envelope-function symmetry despite the small spin-orbit interaction. This is unlike the case in CdS dots, said[25,27] to have a $1pf$ envelope-function symmetry. The difference in predictions arises, most likely, from the simplified assumptions made in the $\mathbf{k}\cdot\mathbf{p}$ calculations of Refs. 25 and 27.

(v) Removal of a cation-passivating atom results in an In dangling-bond state that lies in the gap, below the intrinsic dot conduction band for dot size smaller than 50–60 Å. For larger sizes, the intrinsic conduction state is the lowest unoccupied state. The In dangling-bond state is surface localized, but does not depend much on the identity of the passivating atoms surrounding the dangling bond since this state is made from In orbitals, not from those of the passivant. Thus the fact that spectroscopic properties do not change much as the passivation is altered does not imply the absence of surface effects. The energy of the In DB state changes little with the dot size, but the dipole matrix element between this state and the dot VBM (thus the radiative emission rate)

decreases as the dot becomes larger. The In DB state is related, most likely, to the redshifted emission observed at 1.46 eV of the unetched InP dots and is responsible for the low quantum emission efficiency. Such surface defect states are predicted to show *large* redshifts (~ 500 meV) with a size-dependent (long) radiative lifetime.

(vi) Removal of an anion-passivating atom results in a P dangling-bond state that lies above the intrinsic dot valence band for all dot sizes and has a very weak dipolar coupling to the conduction band. This state is strongly localized and would act as an effective (lifetime shortening) trap for photogenerated holes. This state interacts strongly with the dot intrinsic VBM, shifting it to higher energies (by up to 250 meV) relative to fully passivated dots.

(vii) An analysis of the *sample-averaged* resonant redshift $\tilde{\Delta}(\varepsilon_{\text{excit}})$ observed in selective excitation experiments reveals that it is considerably larger than the inferred *single-dot* redshift $\Delta(\varepsilon_{\text{excit}})$ from which size-distribution effects have been deconvoluted.

(viii) The calculated In dangling-bond state induces a redshift that is too large to explain the observed resonant, single-dot redshift ($\leqslant 20$ meV). It is not impossible that more complex surface chemistry could, however, explain this shift.

(ix) The calculated single-triplet exchange splittings for a *screened* exchange interaction agree well with the observed resonant single-dot redshift. This type of redshift is predicted to be small ($\leqslant 20$ meV) and the redshifted emission has but a weak size dependence of its (long) radiative lifetime.

The effect of vibronic coupling, leading possibly to a change in the equilibrium geometry of the electronically excited dot (and thus to a Frank-Condon-type redshift), was not considered here.

ACKNOWLEDGMENTS

We thank A. Franceschetti, L. W. Wang, and S. B. Zhang for helpful discussions on the theory and O. I. Micic and A. J. Nozik for helpful discussions on their data. This work was supported by the U.S. Department of Energy, OER-BES, under Grant No. DE-AC36-83CH10093.

[1] P. D. J. Calcott, K. J. Nash, L. T. Canham, M. J. Kane, and D. Brumhead, J. Phys. C **5**, L91 (1993).

[2] V. Petrova-Koch, T. Muschik, A. Kux, B. K. Meyer, F. Koch, and V. Lehmann, Appl. Phys. Lett. **61**, 943 (1992).

[3] F. Koch, V. Petrova-Koch, T. Muschik, A. Kux, F. Muller, V. Garilenko, and F. Moller, in *Proceedings of the 21st International Conference on the Physics of Semiconductors, Beijing, 1993*, edited by H. Z. Zheng and P. Jiang (World Scientific, Singapore, 1993), p. 1483.

[4] F. Koch, V. Petrova-Koch, T. Muschik, A. Kux, F. Muller, and V. Garilenko, in *Microcrystalline Semiconductors: Materials Science & Devices*, edited by P. M. Fauchet *et al.*, MRS Symposia Proceedings No. 283 (Materials Research Society, Pittsburgh, 1993), p. 197.

[5] F. Koch, V. Petrova-Koch, and T. Muschik, J. Lumin. **57**, 271 (1993).

[6] Y. Kanemitsu, T. Futagi, T. Matsumoto, and H. Mimura, Phys. Rev. B **49**, 14 732 (1994).

[7] M. G. Bawendi, W. L. Wilson, L. Rothberg, P. J. Carroll, T. M. Jedju, M. L. Steigerwald, and L. E. Brus, Phys. Rev. Lett. **65**, 1623 (1990).

[8] M. G. Bawendi, P. J. Caroll, W. L. Wilson, and L. E. Brus, J. Chem. Phys. **96**, 946 (1992).

[9] D. J. Norris, A. Sacra, C. B. Murray, and M. G. Bawendi, Phys. Rev. Lett. **72**, 2612 (1994).

[10] M. Nirmal, C. B. Murray, and M. G. Bawendi, Phys. Rev. B **50**, 2293 (1994).

[11] D. J. Norris and M. G. Bawendi, J. Chem. Phys. **103**, 5260 (1995).

[12] M. Nirmal, D. J. Norris, M. Kuno, M. G. Bawendi, Al. L. Efros, and M. Rosen, Phys. Rev. Lett. **75**, 3728 (1995).

[13] Al. L. Efros, M. Rosen, M. Kuno, M. Nirmal, D. J. Norris, and M. Bawendi, Phys. Rev. B **54**, 4843 (1996).

[14] M. O'Neil, J. Marohn, and G. Mclendon, J. Phys. Chem. **94**, 4356 (1990).

[15] A. Hasselbarth, A. Eychmuller, and W. Weller, Chem. Phys. Lett. **203**, 271 (1993).

[16] O. I. Micic, J. Sprague, Z. Lu, and A. J. Nozik, Appl. Phys. Lett. **68**, 3150 (1996); O. I. Micic, C. J. Curtis, K. M. Jones, J. R. Sprague, and A. J. Nozik, J. Phys. Chem. **98**, 4966 (1994); O. I. Micic (private communication).

[17] O. I. Micic, M. Cheong, J. Sprague, A. Mascarenhas, H. Fu, A. Zunger, and A. J. Nozik, J. Phys. Chem. (to be published).

[18] S. Fafard, D. Leonard, J. L. Merz, and P. M. Petroff, Appl. Phys. Lett. **65**, 1388 (1994).

[19] M. Grundmann, J. Christen, N. N. Ledentsov, J. Bohrer, D. Bimberg, S. S. Ruvimov, P. Werner, U. Richter, J. Heydenreich, V. M. Ustinov, A. Yu. Egorov, A. E. Zhukov, P. S. Kopev, and Zh. I. Alferov, Phys. Rev. Lett. **74**, 4043 (1995).

[20] T. Takagahara, Phys. Rev. B **47**, 4569 (1993); T. Takagahara and K. Takeda, *ibid.* **53**, R4205 (1996).

[21] U. Woggon, F. Gindele, O. Wind, and C. Klingshirn, Phys. Rev. B **54**, 1506 (1996).

[22] G. L. Bir and G. E. Pikus, *Symmetry and Strain-Induced Effects in Semiconductors* (Wiley, New York, 1975), p. 285.

[23] E. Martin, C. Delerue, G. Allan, and M. Lannoo, Phys. Rev. B **50**, 18 258 (1994).

[24] A. Franceschetti and A. Zunger, Phys. Rev. Lett. **78**, 915 (1997).

[25] T. Richard, P. Lefebvre, H. Mathieu, and J. Allegre, Phys. Rev. B **53**, 7287 (1996).

[26] A. Franceschetti and A. Zunger, Phys. Rev. B **52**, 14 664 (1995); Appl. Phys. Lett. **68**, 3455 (1996).

[27] G. B. Grigoryan, E. M. Kazaryan, Al. L. Efros, and T. V. Yazeva, Fiz. Tverd. Tela (Leningrad) **32**, 1772 (1990) [Sov. Phys. Solid State **32**, 1031 (1990)].

[28] L. W. Wang and A. Zunger, J. Phys. Chem. **98**, 2158 (1994); J. Chem. Phys. **100**, 2394 (1994).

[29] C. Y. Yeh, S. B. Zhang, and A. Zunger, Phys. Rev. B **50**, 14 405 (1994).

[30] C. Delerue, M. Lannoo, and G. Allan, J. Lumin. **57**, 249 (1993).

[31] G. Allan, C. Delerue, and M. Lannoo, Phys. Rev. Lett. **76**, 2961 (1996).
[32] M. A. Tischler, R. T. Collins, J. H. Stathis, and J. C. Tsang, Appl. Phys. Lett. **60**, 639 (1992).
[33] M. S. Brandt and M. Stutzmann, Appl. Phys. Lett. **62**, 2569 (1992).
[34] J. R. Sachleben, E. W. Wooten, L. Emsley, A. Pines, V. L. Colvin, and A. P. Alivisatos, Chem. Phys. Lett. **198**, 431 (1992).
[35] L. Becerra, C. B. Murray, R. G. Griffin, and M. G. Bawendi, J. Chem. Phys. **100**, 3297 (1994).
[36] J. E. Bowen Katari, V. L. Colvin, and A. P. Alivisatos, J. Phys. Chem. **98**, 4109 (1994).
[37] S. A. Majetich, A. C. Carter, J. Belot, and R. D. McCullough, J. Phys. Chem. **98**, 13 705 (1994).
[38] G. Allan, C. Delerue, and M. Lannoo, Phys. Rev. B **48**, 7951 (1993).
[39] Al. L. Efros, Phys. Rev. B **46**, 7448 (1992); Al. L. Efros and A. V. Rodina, *ibid.* **47**, 10 005 (1993).
[40] S. Nomura, Y. Segawa, and T. Kobayashi, Phys. Rev. B **49**, 13 571 (1994).
[41] M. V. Rama Krishna and R. A. Friesner, Phys. Rev. Lett. **67**, 629 (1991); J. Chem. Phys. **95**, 8309 (1991).
[42] V. I. Garilenko, P. Vogl, and F. Koch, in *Microcrystalline Semiconductors: Materials Science & Devices* (Ref. 4), p. 431.
[43] E. V. Tsiper, Phys. Rev. B **54**, 1959 (1996). In Tsiper's model, it is asserted that emission from the lowest excitonic state $|E_{\rm fast}^{(1)}\rangle$ cannot be measured technically when this state is resonantly excited since the emission is masked by the excitation laser beam. Emission from $|E_{\rm fast}^{(1)}\rangle$ is seen in his model only when a *higher* $|E_{\rm fast}^{(2)}\rangle$ state is excited. Hence the redshift is simply $E_{\rm fast}^{(2)}-E_{\rm fast}^{(1)}$. This model overlooks the fact that even in a dot, state $|E_{\rm fast}^{(1)}\rangle$ has a finite (although narrow) spectral width, so one can tune the absorption to occur at a slightly different wavelength from the emission. Furthermore, time-resolved experiments avoid the technical difficulty of ''masking'' by using fast excitation pulses that vanish long before the emission occurs. Finally, Tsiper's model does not explain the issue of the observed long lifetime of the lowest emitting state.
[44] L. W. Wang and A. Zunger, Phys. Rev. B **51**, 17 398 (1995).
[45] H. Fu and A. Zunger, Phys. Rev. B **55**, 1642 (1997).
[46] M. L. Cohen and T. K. Bergstresser, Phys. Rev. **141**, 789 (1966).
[47] ftp to ftp.nrel.gov as anonymous, change directory to pub/sst-out/InP.SEPM, and download the files there.
[48] T. Chasse, G. Neuhold, and K. Horn, Surf. Sci. **331–333**, 511 (1995); A. Tulke and H. Luth, *ibid.* **211/212**, 1001 (1989); A. Huijser, J. v. Laar, and T. L. v. Rooy, *ibid.* **62**, 472 (1977).
[49] For cubic dots, we prefer this definition to $d=(3N/4\pi)^{1/3}a$ used in Ref. 28 for other dots including spherical ones.
[50] L. W. Wang and A. Zunger, in *Nanocrystalline Semiconductor Materials*, edited by P. V. Kamat and D. Meisel (Elsevier, Amsterdam, 1996), p. 161.
[51] N. A. Hill and K. B. Whaley, Phys. Rev. Lett. **75**, 1130 (1995).
[52] L. W. Wang and A. Zunger, Phys. Rev. B **53**, 9579 (1996).
[53] L. E. Brus, J. Phys. Chem. **90**, 2555 (1986).
[54] G. W. Bryant, Phys. Rev. B **37**, 8763 (1988).
[55] F. Bassani and G. Pastori Parravivini, *Electronic States and Optical Transitions in Solids* (Pergamon, Oxford, 1985), p. 175.
[56] R. Resta, Phys. Rev. B **16**, 2717 (1977).
[57] L. W. Wang and A. Zunger, Phys. Rev. Lett. **73**, 1039 (1994).
[58] R. Tsu and D. Babic, Appl. Phys. Lett. **64**, 1806 (1994).
[59] Our calculated energy levels for V_P^0 in InP are $\epsilon(a_1)=\epsilon_{\rm VBM}+0.06$ eV and $\epsilon(t_2)=\epsilon_{\rm VBM}+1.75$ eV. These can be compared with the previously calculated values $\epsilon(a_1)=\epsilon_{\rm VBM}+0.28$ eV, $\epsilon(t_2)=\epsilon_{\rm VBM}+1.50$ eV [from Ref. 60 using the tight-binding (TB) method], $\epsilon(a_1)=\epsilon_{\rm VBM}+0.07$ eV, $\epsilon(t_2)=\epsilon_{\rm VBM}+1.64$ eV (from Ref. 61 using the TB method), and $\epsilon(a_1)=\epsilon_{\rm VBM}+0.12$ eV (from Ref. 62 using the atomic orbital energy). Generally, the charge redistribution due to the presence of a vacancy cannot be described by a bulk-fitted pseudopotential. In order to describe such charge redistribution effects, we have carried out a self-consistent LDA calculation for the neutral vacancy in the bulk and we added to our SEPM potential near the vacant site an additional term so that the vacancy level shift is fitted to the LDA results. This adjustment accounts for the effect of charge self-consistency to first order in perturbation.
[60] D. N. Talwar and C. S. Ting, Phys. Rev. B **25**, 2660 (1982).
[61] H. Xu, Phys. Rev. B **42**, 11 295 (1990).
[62] A. Madhukar and S. Das Sarma, J. Vac. Sci. Technol. **1**, 1120 (1980).
[63] P. J. Lin-chung and T. L. Reincheck, Phys. Rev. B **27**, 1101 (1983).
[64] G. Allan and M. Lannoo, Surf. Sci. **63**, 11 (1977).
[65] Our values for $V_{\rm In}^0$ in InP of $\epsilon(a_1)=\epsilon_{\rm VBM}-0.73$ eV and $\epsilon(t_2)=\epsilon_{\rm VBM}+0.39$ eV can be compared with $\epsilon(t_2)=\epsilon_{\rm VBM}+0.54$ eV (Ref. 60), $\epsilon(t_2)=\epsilon_{\rm VBM}+0.24$ eV (Ref. 61), and $\epsilon(a_1)=\epsilon_{\rm VBM}-0.55$ eV and $\epsilon(t_2)=\epsilon_{\rm VBM}+0.44$ eV (Ref. 63).
[66] Here we neglect the Coulomb interaction between an electron in the In DB state and a hole in the VBM because of the small wave-function overlap between these states.
[67] We found that the log-normal function of the size distribution used in Ref. 16 can be extremely well described by the Gaussian function. Therefore, we here use the common Gaussian function instead of the log-normal function.
[68] Note that, even though the position of the energy level of an In DB state (Fig. 6) may be shifted by scaling our potential (e.g., due to self-consistency effects neglected here), this does not change the *slope* of the redshift vs gap in Fig. 5.